(Preprint) AAS 22-569

CONCURRENT OPTIMIZATION OF GRAVITY-ASSIST LOW-THRUST TRAJECTORY WITH POWER AND PROPULSION SUBSYSTEM SIZING

Yuri Shimane,[*] Dyllon Preston,[†] and Koki Ho[‡]

Low-thrust technology is a key driver in current and upcoming space exploration missions due to their high specific impulse. A challenge when designing low-thrust trajectories is due to the inherent coupling of the power and propulsion subsystems with the trajectory, as the spacecraft mass greatly affect the obtainable acceleration by a given propulsion subsystem. To this end, this work proposes an approach for coupling the sizing process of the power and propulsion subsystems to a direct-transcription-based trajectory optimization problem, which enables a concurrent trade-space exploration of both the trajectory and the spacecraft design.

INTRODUCTION

With recent advances in electric propulsion (EP) technology, exploration of our solar system neighborhood has become far more accessible. EP's characteristically high specific impulse (I_{sp}) enables larger payload fraction to be delivered, directly translating to more scientific outcome. In contrast to chemical thrusters, EP systems achieve their high I_{sp} by accelerating their propellant to high exhaust velocities, which leads to large power consumption. For spacecraft applications, such large power requirement becomes a driving constraint on the power subsystem as well as the spacecraft as a whole. To meet such power-hungry requirements, a traditional approach has been to use radioisotope thermoelectric generator (RTG) such as NASA's MMRTG[1] for missions to the outer-solar system. However, recent developments in solar electric systems have opened ways for the use of solar-based power systems in such missions as well. Such solar electric propulsion (SEP) based missions include Deep Space 1, Dawn, Hayabusa 1 and 2,[2,3] BepiColombo,[4,5] Psyche,[6] and DESTINY+.[7] Table 1 shows a summary of past, present, and future SEP missions exploring the solar system.

On top of the aforementioned design constraint placed by the power requirements, with the radial and time dependence of the available power from a given solar electric system, the coupling of a trajectory for a SEP spacecraft with its power and propulsion subsystems cannot be neglected. Adding further complexity to the trajectory design is the multiple operational settings at which an EP system may be operated; these settings typically lead to thrust and I_{sp} being nonlinear functions of power consumption. In such scenario, the optimal trajectory of an EP spacecraft may involve operating the thruster at differing settings along its transfer.

*PhD Student, School of Aerospace Engineering, Georgia Institute of Technology, Atlanta, GA 30332.
†Undergraduate Student, School of Aerospace Engineering, Georgia Institute of Technology, Atlanta, GA 30332.
‡Assistant Professor, School of Aerospace Engineering, Georgia Institute of Technology, Atlanta, GA 30332.

Table 1: Key figures from interplanetary missions employing solar electric propulsion

Mission	Destination	Destination SMA, AU	Wet mass, kg	Power at 1 AU, kW	Thrusters
Deep Space 1	9969 Braille	2.341	486	2.5	$1\times$ NSTAR
Dawn	1 Ceres	2.768	1217	10	$3\times$ NSTAR
Hayabusa	25143 Itokawa	1.324	510	2.6	$4\times$ μ10
Hayabusa 2	162173 Ryugu	1.190	610	2.6	$4\times$ μ10
BepiColombo	Mercury	0.387	4100	14	$4\times$ QinetiQ T6
Psyche	16 Psyche	2.921	2608	20	$4\times$ SPT-140
DESTINY+	3200 Phaethon	1.271	480	4.7	$4\times$ μ10

As exploration of planets such as Venus and Mars as well as asteroids gain increasing attention,[8] a method for concurrently optimizing the trajectory along with the relevant subsystems of a SEP spacecraft is pertinent. In the context of space mission planning and vehicle design, Isaji et al[9] considered an optimization problem with concurrent subsystem sizing, however only a fixed option for the trajectories have been considered. Recent literature on simultaneous design of spacecraft trajectory and system includes Nicholas et al,[10] which decoupled the spacecraft sizing and trajectory design problems, and optimized these individually while ensuring that the mission as a whole (i.e. combination of spacecraft and its trajectory) to be feasible. Petukhov and Sang Wook[11] studied the joint optimization of key parameters of the propulsion and power subsystems for optimizing nuclear electric propulsion trajectories via optimal control theory. Arya et al[12] later studied the trajectory design as an optimal control problem via a Composite Smoothing Control framework, with the power at beginning of life (BOL) as part of the state variables. In the context of Earth-based satellites, Ceccherini et al[13] studied the combined optimization of a GEO spacecraft and its transfer trajectory from injection by the launcher. Trajectory design with varying thruster mode has also been studied; Taheri[14] and Arya et al[15] considered discrete thruster modes simultaneously.

In this work, the low-thrust trajectory design and the subsystem sizing are considered simultaneously as a single optimization problem that can be solved by gradient-based optimization algorithms. Leveraging on the success of direct methods in conducting efficient trade-space search for spacecraft trajectories, this work extends this capability by incorporating key parameters of SEP spacecraft into the direct method-based trajectory optimization problem. Specifically, the power and propulsion subsystems are parameterized through a combination of previously adopted models and a novel interpolation scheme for sizing thrusters. The proposed method provides an effective tool for conducting architecture and trajectory trade-studies concurrently.

The paper is organized as follows: initially, the Sims-Flanagan Transcription, a direct method based trajectory optimization scheme, which forms the basis of the problem in this work, is introduced. Then, the model used to decompose the spacecraft is introduced. This also involves a discussion on the way in which the propulsion unit is scaled, based on data from existing EP systems. This is followed by a description on the integration of the spacecraft model into the trajectory design problem, resulting in the extend problem formulation. The introduced approach is employed for a case-study of a cargo mission to Mars.

OVERVIEW OF DIRECT LOW-THRUST TRAJECTORY OPTIMIZATION

The traditional Sims-Flanagan Transcription (SFT) problem[16–18] decomposes a gravity-assist trajectory into a sequence of N legs, each beginning and ending at a node. The node typically represents a departure, fly-by, or arrival at a celestial body, while it is not limited to these and may just be a user-defined state osculating in time. Within each leg, the spacecraft state $\boldsymbol{y} = [\boldsymbol{r}, \boldsymbol{v}, m]^{\mathrm{T}}$ is propagated forward from the earlier node and backward from the latter node. The mismatch of the spacecraft state at the end of the forward and backward propagation is incorporated as an equality constraint, denoted as $\boldsymbol{h}_{\mathrm{mp}}$, given by

$$\boldsymbol{h}_{\mathrm{mp}}^{i} = \boldsymbol{y}_{\text{backward}}^{i} - \boldsymbol{y}_{\text{forward}}^{i}\,, \quad i = 1, \ldots, N \tag{1}$$

The propagation is typically done by discretization of the forward and backward portion of the leg to segments, where each segment approximates the net effect of continuous, low-thrust acceleration via a single impulse at the center of the segment. The total number of segments of the i^{th} leg is denoted as n^{i}. For detailed illustration of this implementation, see Shimane and Ho.[19]

The objective of a trajectory optimization problem typically involves the mass, time of flight, or some combination of the two. In this work, since the purpose is to explore a wide range of spacecraft architecture for achieving payload delivery to a given destination, a minimization of an aggregated sum of the initial mass at LEO, denoted as IMLEO ("Initial Mass at LEO"), and the time of flight, is considered; thus, the objective function f is given by

$$f(\boldsymbol{x}) = w_1 \mathrm{IMLEO} + w_2 \mathrm{TOF}_{\max} \tag{2}$$

where $\boldsymbol{x}$ is the decision vector, and w_i are the weights on each objective term. In addition, an inequality constraint on the total time of flight is imposed to restrict the design space when the optimizer attempts to prioritize the minimization of the IMLEO

$$g_{\text{TOF}} = \sum_{i=0}^{N} \Delta t_i - \mathrm{TOF}_{\max} \leq 0 \tag{3}$$

In the case of planetary gravity assists, an additional constraint must be enforced to ensure the spacecraft does not intersect with a safety sphere around the planet, defined by a safety radius. This constraint takes the form

$$\boldsymbol{g}_{\text{gravity-assist}} = \left(r_{\text{planet}} + h_{\text{safe}}\right) - \frac{\mu_{\text{planet}}}{v_{\infty}^{2}} \left[1/\sin\left(\frac{\delta_{\text{turn-angle}}}{2}\right) - 1\right] \leq 0 \tag{4}$$

where $\delta_{\text{turn-angle}}$ is obtained by

$$\delta_{\text{turn-angle}} = \arccos\left(\frac{\boldsymbol{v}_{\infty}^{-} \cdot \boldsymbol{v}_{\infty}^{+}}{v_{\infty}^{-} v_{\infty}^{+}}\right) = \arccos\left(\frac{\boldsymbol{v}_{\infty}^{-} \cdot \boldsymbol{v}_{\infty}^{+}}{v_{\infty}^{2}}\right) \tag{5}$$

The resulting optimization problem is given by

$$\begin{aligned} \min_{\boldsymbol{x}} \quad & \text{eqn. (2)} \\ \text{s.t.} \quad & \boldsymbol{h}_{\mathrm{mp}}(\boldsymbol{x}) = 0 \\ & g_{\mathrm{TOF}}(\boldsymbol{x}) \leq 0 \\ & \boldsymbol{g}_{\text{gravity-assist}}(\boldsymbol{x}) \leq 0 \end{aligned} \tag{6}$$

In traditional SFT problems, the value of IMLEO is simply taken as the initial mass m^0 of the spacecraft. The decision vector $\boldsymbol{x}$ for a traditional SFT problem takes the form

$$\boldsymbol{x} = [\boldsymbol{c}_{\text{departure}},\, \boldsymbol{c}^{1}_{\text{gravity-assist}},\, \ldots,\, \boldsymbol{c}^{N-1}_{\text{gravity-assist}},\, \boldsymbol{c}_{\text{arrival}},\, \boldsymbol{\tau}^{1},\, \ldots,\, \boldsymbol{\tau}^{N}]^{\mathrm{T}} \tag{7}$$

where $\boldsymbol{c}$ is a collection of optimization variables of nodes, while $\boldsymbol{\tau}$ is a collection of thrust controls of each leg. The node variables $\boldsymbol{c}$ are given by

$$\boldsymbol{c}_{\text{type}} = \begin{cases} \left[t_0, m^0, v^1_\infty, \alpha^1, \delta^1\right] & \text{if type is departure} \\ \left[\Delta t^i, m^i, v^{i+1}_\infty, \alpha^{i+1}_-, \delta^{i+1}_-, \alpha^{i+1}_+, \delta^{i+1}_+\right],\ i \in [1, N-1] & \text{if type is gravity-assist} \\ \left[\Delta t^N, v^{N+1}_\infty, \alpha^{N+1}, \delta^{N+1}\right] & \text{if type is arrival} \end{cases} \tag{8}$$

where t_0 is the departure epoch, Δt is the duration of a leg, and α and δ are the right-ascension and declination angles with respect to a celestial body, and m is the spacecraft mass at the encounter with the celestial body. The subscripts $(\cdot)_-$ and $(\cdot)_+$ on α and δ indicate incoming and outgoing values when the spacecraft undergoes a gravity-assist. The superscripts denote the i^{th} value of the specific type of variable. Note that the final node $\boldsymbol{c}_{\text{arrival}}$ does not have an associated mass variable, since the final mass corresponds to the sum of the spacecraft bus and payload mass, which is considered to be fixed. The thrust control variables $\boldsymbol{\tau}$ are given by

$$\boldsymbol{\tau}^i = [\tau_{i,1}, \ldots, \tau_{1,n}, \theta_{i,1}, \ldots, \theta_{i,n}, \beta_{i,n}, \ldots, \beta_{i,n}] \tag{9}$$

where $\tau \in [0, 1]$ is the duty cycle of the thruster, $\theta \in [-\pi, \pi]$ is the in-plane angle, and $\beta \in [-\pi/2, \pi/2]$ is the out-of-plane angle of the thrust vector in the local-vertical-local-horizontal frame (LVLH). The resulting impulsive ΔV vector on the j^{th} segment is given by

$$\Delta \boldsymbol{v}_{i,j} = \tau_{i,j} \frac{T}{m} \Delta t_{\text{seg}} \boldsymbol{T}_{\text{EL}}(\boldsymbol{r}, \boldsymbol{v}) \left[\cos(\theta_{i,j}) \cos(\beta_{i,j}),\, \sin(\theta_{i,j}) \cos(\beta_{i,j}),\, \sin(\beta_{i,j})\right]^{\mathrm{T}} \tag{10}$$

where T is the thrust, Δt_{seg} is the duration of the segment, and the 3 by 3 matrix $\boldsymbol{T}_{\text{EL}}(\boldsymbol{r}, \boldsymbol{v})$ transforms the vector from the LVLH frame into the inertial frame. Together with the velocity, the mass is also modified impulsively via

$$\Delta m_{i,j} = -\tau_{i,j} \dot{m} \Delta t_{\text{seg}} \tag{11}$$

where $\Delta m_{i,j}$ is the change in mass, and $\dot{m}$ is the mass-flow rate.

SPACECRAFT MODELING

In order to capture the design parameters of the spacecraft that are directly coupled with the trajectory, the subsystem-decomposition by Petukhov et al[11] is adopted. The model consists of decomposing the spacecraft mass into the useful mass m_u, the mass of the power supply and propulsion unit (PSPU) m_{PSPU}, and the mass of the power storage and feeding system (PSFS) m_{PSFS}. Hence, the IMLEO is expressed as

$$\text{IMLEO} = m_u + m_{\text{PSPU}} + m_{\text{PSFS}} \tag{12}$$

The useful mass consists of the payload as well as the primary subsystems of the spacecraft bus that does not concern the electric propulsion system (EPS). The EPS, on the other hand, consists of the PSPU and the PSFS.

The PSPU consists of the power-supply system, PPU for the EPS, and the thrusters. The PSPU mass can be expressed as

$$m_{\text{PSPU}} = \gamma_1 P_{\text{BOL}} + \gamma_2 s P_{\text{EPS}}^{\text{max}} \tag{13}$$

where P_{BOL} is the power produced by the SA at the beginning of life (BOL), and $P_{\text{EPS}}^{\text{max}}$ is the maximum power handled by a reference propulsion system, and s is a scalar to model variable propulsion systems, which will be further explained in the Propulsion Subsystem Modeling section. The coefficient γ_1 is the specific mass of the solar arrays (SA) in kg/kW, and γ_2 is the specific mass of the power regular unit, the part of the solar array drives of the PSS used for the EPS as well as the EPS itself in kg/kW.

The PSFS mass is given by

$$m_{\text{PSFS}} = m_{\text{propellant}}^0 (1 + a_t) \tag{14}$$

where a_t is the ratio of tank to initial propellant mass.

Substituting these expressions back into (12),

$$\text{IMLEO} = m_u + \gamma_1 P_{\text{BOL}} + \gamma_2 s P_{\text{EPS}}^{\text{max}} + m_{\text{propellant}}^0 a_t + m_{\text{propellant}}^0 \tag{15}$$

Note that the PSFS term has been expanded out to isolate the last propellant mass; now, the mass of the spacecraft at time t along the mission can be expressed as

$$m(t) = m_u + \gamma_1 P_{\text{BOL}} + \gamma_2 s P_{\text{EPS}}^{\text{max}} + m_{\text{propellant}}^0 a_t + m_{\text{propellant}}(t) \tag{16}$$

where $m_{\text{propellant}}(t)$ is the remaining propellant mass at time t.

Power Subsystem Modeling

Due to the radial dependence of the available solar power and the inherent degradation of power cells, the power delivered by the solar arrays is a function of both the radius r and elapsed time t

$$P_{\text{generated}}(r(t), t) = \min\left(\frac{P_{\text{BOL}}}{r^2} \left[\frac{d_1 + d_2 r^{-1} + d_3 r^{-2}}{1 + d_4 r + d_5 r^2} \right] \left(\frac{100 - D}{100} \right)^t, P_{\text{solar-array}}^{\text{max}} \right) \tag{17}$$

where D is the degradation rate, in units $\%/\text{year}$, and $P_{\text{solar-array}}^{\text{max}}$ is an upper-bound on the power generated due to component's limitations. While the propulsion system is the most power-hungry component in a SEP spacecraft, a portion of the power must also be diverted to other purposes on the spacecraft bus. The power available to the propulsion system is thus given by

$$P_{\text{propulsion}}^{\text{available}} = \begin{cases} \min(P_{\text{EPS}}^{\text{max}}, P_{\text{ppu}}^{\text{max}}) & \text{if } P_{\text{generated}} \geq P_L + P_{\text{ppu}}^{\text{max}} \\ \min(P_{\text{EPS}}^{\text{max}}, (P_{\text{generated}} - P_L)) & \text{if } P_{\text{generated}} < P_L + P_{\text{ppu}}^{\text{max}} \end{cases} \tag{18}$$

where P_L is the power required to operate the spacecraft bus and payload.

Propulsion Subsystem Modeling

The propulsion subsystem is modeled by scaling a reference thruster performance profile, and a propellant tank that is assumed to scale in mass with the required amount of propellant via a scaling factor a_t.

Thruster Modeling The thruster performance can typically be modeled as polynomials of the power used by the thruster.[20] In particular, third-order polynomials are used such that

$$T(P_{\text{propulsion}}) = c_{T,0} + c_{T,1}P_{\text{propulsion}} + c_{T,2}P^2_{\text{propulsion}} + c_{T,3}P^3_{\text{propulsion}} \tag{19}$$

$$\dot{m}(P_{\text{propulsion}}) = c_{\dot{m},0} + c_{\dot{m},1}P_{\text{propulsion}} + c_{\dot{m},2}P^2_{\text{propulsion}} + c_{\dot{m},3}P^3_{\text{propulsion}} \tag{20}$$

In this work, the NEXT thruster currently in development by NASA Goddard Space Flight Center[21,22] is modeled using third-order polynomials.

Thruster Scaling Given the performance profile of a thruster as a polynomial, the capability of the propulsion system is scaled by the optimizer through a scalar variable s. A scaled polynomial $q_s(\cdot)$ is given by

$$q_s(p) = \begin{cases} 0 & \text{if } p < sP^{\text{min}}_{\text{EPS}} \\ sq\left(\frac{p}{s}\right) & \text{if } sP^{\text{min}}_{\text{EPS}} \leq p \leq sP^{\text{max}}_{\text{EPS}} \\ sq\left(\frac{sP^{\text{max}}_{\text{EPS}}}{s}\right) & p > sP^{\text{max}}_{\text{EPS}} \end{cases} \tag{21}$$

where $q(\cdot)$ is the polynomial representing the thrust or mass flow-rate, given by expressions (19) or (20) respectively, such that

$$\tilde{T}(P_{\text{propulsion}}) = \begin{cases} 0 & \text{if } p < sP^{\text{min}}_{\text{EPS}} \\ sT\left(\frac{p}{s}\right) & \text{if } sP^{\text{min}}_{\text{EPS}} \leq p \leq sP^{\text{max}}_{\text{EPS}} \\ sT\left(\frac{sP^{\text{max}}_{\text{EPS}}}{s}\right) & p > sP^{\text{max}}_{\text{EPS}} \end{cases} \tag{22}$$

$$\tilde{\dot{m}}(P_{\text{propulsion}}) = \begin{cases} 0 & \text{if } p < sP^{\text{min}}_{\text{EPS}} \\ s\dot{m}\left(\frac{p}{s}\right) & \text{if } sP^{\text{min}}_{\text{EPS}} \leq p \leq sP^{\text{max}}_{\text{EPS}} \\ s\dot{m}\left(\frac{sP^{\text{max}}_{\text{EPS}}}{s}\right) & p > sP^{\text{max}}_{\text{EPS}} \end{cases} \tag{23}$$

Figures 1 and 2 show the variation of the thrust and mass-flow rate profile against power, for values of s ranging between 1 and 10. In the case of $s = 1$, the profile corresponds to a single NEXT thruster. The actual power used by the propulsion system, p, is allowed to vary at each segment along a leg based on a power setting parameter $\eta_{i,j}$, such that

$$p_{i,j} = \eta_{i,j} P^{\text{available}}_{\text{propulsion}} \tag{24}$$

where $p_{i,j}$ is the power used on the i^{th} leg during the j^{th} segment.

EXTENDED PROBLEM FORMULATION

Taking into account the propulsion and power subsystem models, the decision vector to the optimization problem outlined in (6) becomes

$$\tilde{\boldsymbol{x}} = \left[\tilde{\boldsymbol{c}}_{\text{departure}},\, \tilde{\boldsymbol{c}}^1_{\text{gravity-assist}},\, \dots,\, \tilde{\boldsymbol{c}}^{N-1}_{\text{gravity-assist}},\, \tilde{\boldsymbol{c}}_{\text{arrival}},\, \tilde{\boldsymbol{\tau}}^1,\, \dots,\, \tilde{\boldsymbol{\tau}}^N,\, P_{\text{BOL}}, s\right]^{\text{T}} \tag{25}$$

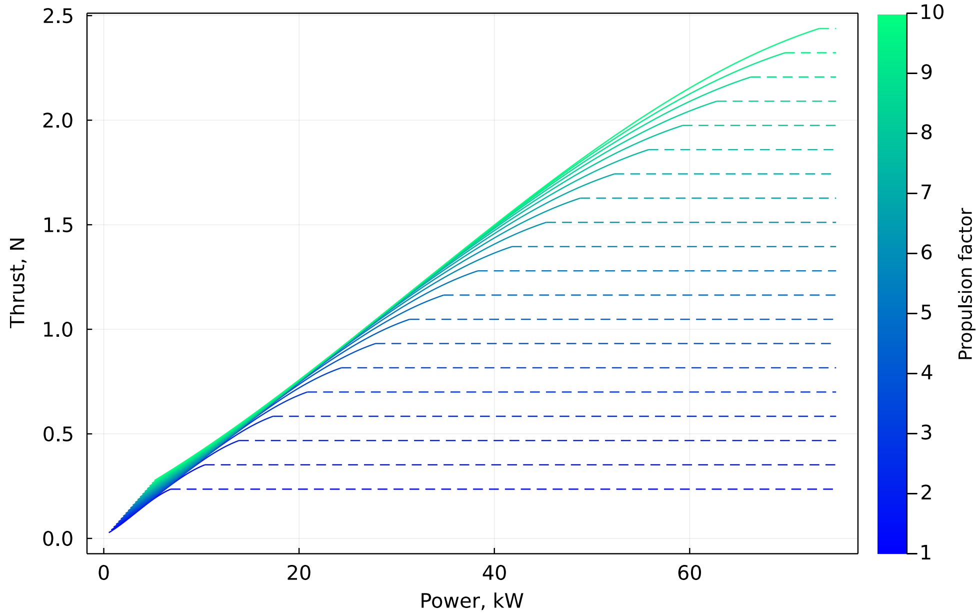

Figure 1: Variation of thrust against power for varying propulsion factor s

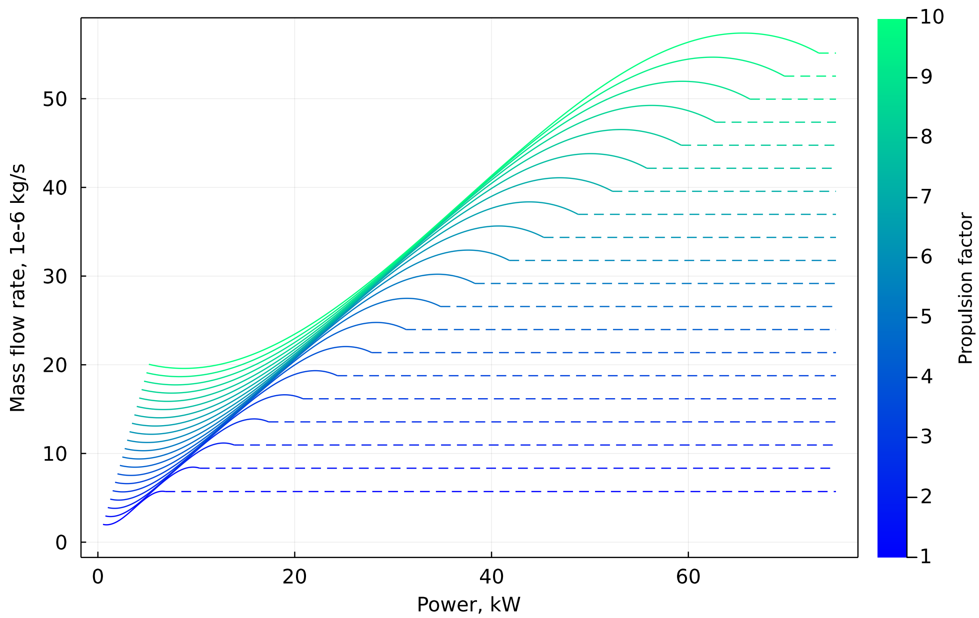

Figure 2: Variation of mass-flow rate against power for varying propulsion factor s

where the modified node variables $\tilde{\boldsymbol{c}}$ are given by

$$\tilde{\boldsymbol{c}}_{\text{type}} = \begin{cases} \left[t_0, m^0_{\text{propellant}}, \gamma_{v^1_\infty}, \alpha^1, \delta^1\right] & \text{if type is departure} \\ \left[\Delta t^i, m^i_{\text{propellant}}, v^{i+1}_\infty, \alpha^{i+1}_-, \delta^{i+1}_-, \alpha^{i+1}_+, \delta^{i+1}_+\right],\ i \in [1, N-1] & \text{if type is gravity-assist} \\ \left[\Delta t^N, v^{N+1}_\infty, \alpha^{N+1}, \delta^{N+1}\right] & \text{if type is arrival} \end{cases} \tag{26}$$

The difference appears at the mass variable, where the remaining propellant mass rather than the entire spacecraft mass is tuned by the optimizer. Note that since no propellant mass is left at arrival, $\tilde{\boldsymbol{c}}_{\text{arrival}}$ is identical to $\boldsymbol{c}_{\text{arrival}}$. The modified thrust control variables $\tilde{\boldsymbol{\tau}}$ are given by

$$\tilde{\boldsymbol{\tau}}^i = [\tau_{i,1}, \ldots, \tau_{i,n}, \theta_{i,1}, \ldots, \theta_{i,n}, \beta_{i,n}, \ldots, \beta_{i,n}, \eta_{i,1}, \ldots, \eta_{i,n}] \tag{27}$$

Now, the expressions for the impulsive Δv's and Δm from expressions (10) and (11) are modified to include implicit dependence on $p_{i,j}$

$$\Delta \boldsymbol{v}_{i,j} = \tau_{i,j} \frac{T(p_{i,j})}{m} \Delta t_{\text{seg}} \boldsymbol{T}_{\text{EL}}(\boldsymbol{r}, \boldsymbol{v}) \left[\cos(\theta_{i,j})\cos(\beta_{i,j}),\ \sin(\theta_{i,j})\cos(\beta_{i,j}),\ \sin(\beta_{i,j})\right]^{\text{T}} \tag{28}$$

$$\Delta m_{i,j} = -\tau_{i,j} \dot{m}(p_{i,j}) \Delta t_{\text{seg}} \tag{29}$$

where $T(p_{i,j})$ is the thrust polynomial based on expression (22), and $\dot{m}(p_{i,j})$ is the mass-flow rate polynomial based on expression (23).

By considering the spacecraft mass breakdown according to equation (12), the spacecraft mass at the encounter with the i^{th} body is given by

$$m^i = \begin{cases} m_u + \gamma_1 P_{\text{BOL}} + \gamma_2 s P^{\text{max}}_{\text{EPS}} + m^0_{\text{propellant}} a_t + m^{i-1}_{\text{propellant}} & 1 \leq i \leq N \\ m_u + \gamma_1 P_{\text{BOL}} + \gamma_2 s P^{\text{max}}_{\text{EPS}} + m^0_{\text{propellant}} a_t & i = N+1 \end{cases} \tag{30}$$

In summary, the optimization problem is given by

$$\begin{aligned} \min_{\tilde{\boldsymbol{x}}} \quad & \text{eqn. (2)} \\ \text{s.t.} \quad & \boldsymbol{h}_{\text{mp}}(\tilde{\boldsymbol{x}}) = 0 \\ & g_{\text{TOF}}(\tilde{\boldsymbol{x}}) \leq 0 \\ & \boldsymbol{g}_{\text{gravity-assist}}(\tilde{\boldsymbol{x}}) \leq 0 \end{aligned} \tag{31}$$

OPTIMIZATION METHOD

Due to the highly constrained nature of the problem at hand, gradient-based methods are known to be suitable for driving an initial guess that likely violates some if not all the constraints, to a feasible, local optimal solution. As such, well-established routines such as SNOPT[23] and IPOPT[24] are useful in this type of problems. One drawback to keep in mind when using gradient-based solvers is the fact that these converge to local optimal solutions, within a design-space that contains multiple, isolated clusters of these local optima. To overcome this challenge, Monotonic Basin Hopping (MBH), a pseudo-algorithm initially introduced by Wales and Doye[25] that wraps local optimal solvers and performs global search, has been found to be particularly effective by multiple authors for interplanetary trajectory design problems, and is also employed in this work.[26–30]

Table 2: Earth-Mars Cargo Mission Parameters

Parameter	Value
Earliest launch date, UTC	2030-01-01 00:00:00.00
Latest launch date, UTC	2033-03-01 00:00:00.00
Maximum Time of Flight, year	3
Useful mass, kg	5000
Base thruster	NEXT
Bounds on s	$[1, 10]$
Max departure v_∞, $\mathrm{km/s}$	2.0
Max arrival v_∞, $\mathrm{km/s}$	0.0
γ_1	10
γ_2	15
a_t	0.1
Objective weights w_1, w_2	$1, 1$

RESULTS

The proposed method for formulating the concurrent optimization problem is implemented in Julia, leveraging a set of codes previously developed by the authors.[19,30] This is tested for an Earth-Mars cargo mission scenario, where an aggregate objective function of the IMLEO and time of flight is considered to explore the possible design space of the spacecraft together with the trajectories. This problem is solved using MBH together with SNOPT.

Case Study: Earth-Mars Cargo Mission

The scenario consists of a cargo mission to deliver a $5000\,\mathrm{kg}$ useful mass to Mars at a rendezvous velocity of $0\,\mathrm{km/s}$ with a direct transfer from Earth. The mission parameters are summarized in Table 2. Values for γ_1, γ_2 and a_t are due to Arya et al.[15]

Figure 3 shows the Pareto front of the time of flight against the required IMLEO. Due to expression (15), the IMLEO scales linearly with $P_{\mathrm{EPS}}^{\max}$, which in turn scales linearly with the propulsion factor s. This is clearly visible from the color scale, where propulsion factor increases as IMLEO increases. Analyses with the same axes in Figure 3 appears commonly in mission analysis literature, as a trade-off tool between IMLEO and TOF. However, the present plot also provides an additional design dimension, where trajectories corresponding to each point on the plot do not necessarily correspond to the same spacecraft architecture. Note also that due to the nature of the low-thrust trajectory optimization containing many local minima, there are many non-dominant solutions that have been detected. The trade-off of interest is at the lower-left corner of the Figure, where the time of flight may be traded-off with IMLEO. Specifically, it is possible to observe an initial trend of decreasing TOF with increasing IMLEO due to increasing propulsion factor. This region corresponds to solutions achieving faster transfers due to the increasing capability of the propulsion system. Then, beyond an IMLEO of around $7400\,\mathrm{kg}$, the TOF starts to increase again for increasing IMLEO. Here, the design space corresponds to a region where as the propulsion factor increases, the propulsion system becomes prohibitively heavy and the increase in achievable acceleration does not balance out the additional inertia, thus leading to longer TOF.

With the formulation introduced, it is also possible to identify the optimal subsystem sizes neces-

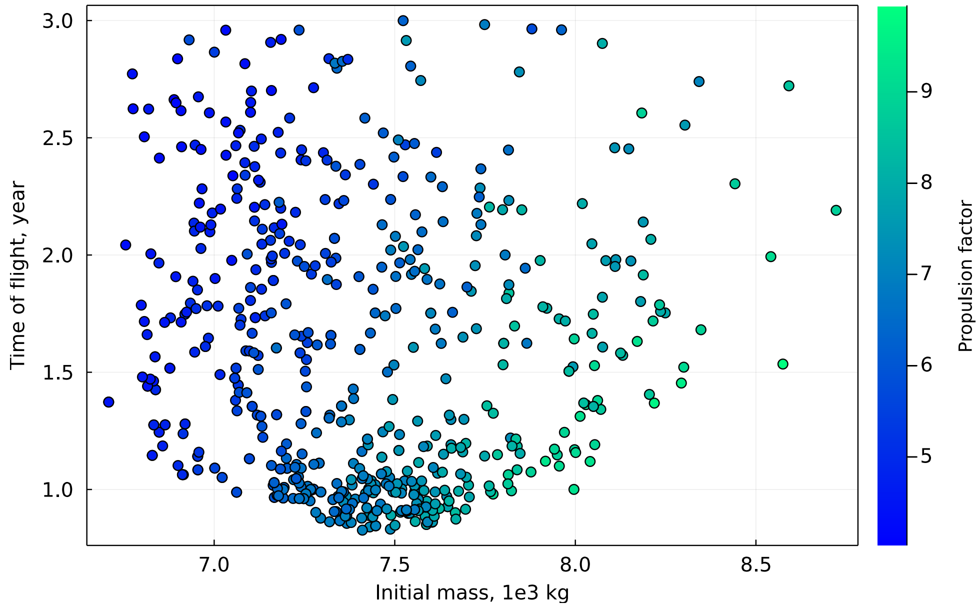

Figure 3: Pareto front of time of flight and IMLEO

Table 3: Summary of IMLEO-optimal and TOF-optimal solutions

Solution	Launch epoch, UTC	Arrival epoch, UTC	Time of flight, day	Initial mass, kg	Final mass, kg	Propulsion Factor
Min-IMLEO solution	2030-11-21 09:02:26.435	2032-04-05 19:12:35.811	501.42	6707.93	5892.58	4.4806
Min-TOF solution	2033-03-01 00:00:00.000	2033-12-27 21:50:18.562	301.91	7146.35	6296.08	7.0466

sary to minimize classic trajectory design objectives, such as IMLEO and TOF. Figure 4 shows the IMLEO against the propulsion factor, where the minimizing solution is found to have $s \approx 4.5$. Due to the linear contribution of s on the IMLEO as given in equation (15), the relationship between the IMLEO and s is generally linear, as it is visible from this Figure. However, the contribution of the propellant to achieve an Earth-Mars transfer must also be taken into account, and this is not necessarily a linear scaling; a larger propulsion system would require larger amount of propellant to achieve its full thrust, but require less burn time to provide the spacecraft with a certain amount of acceleration. As a result, the minimum IMLEO solution isn't achieved with the minimum s solution. It is also possible to observe generally similar TOF solutions (similar color scale) along the diagonal direction of both increasing IMLEO and propulsion factor.

In contrast to Figure 4, from Figure 5, the solution that minimizes the time of flight is found with $s \approx 7.2$. This is again a result of the trade-off between propulsion systems that provide more thrust but has a heavier penalty on the IMLEO, corresponding to larger s, against propulsion systems that provide less thrust but is lighter, corresponding to smaller s; $s \approx 7.2$ corresponds to the balance that has been found to minimize TOF. Table 3 shows key variables of the minimum-IMLEO and minimum-TOF solutions, respectively, and Figure 6 shows the corresponding trajectories.

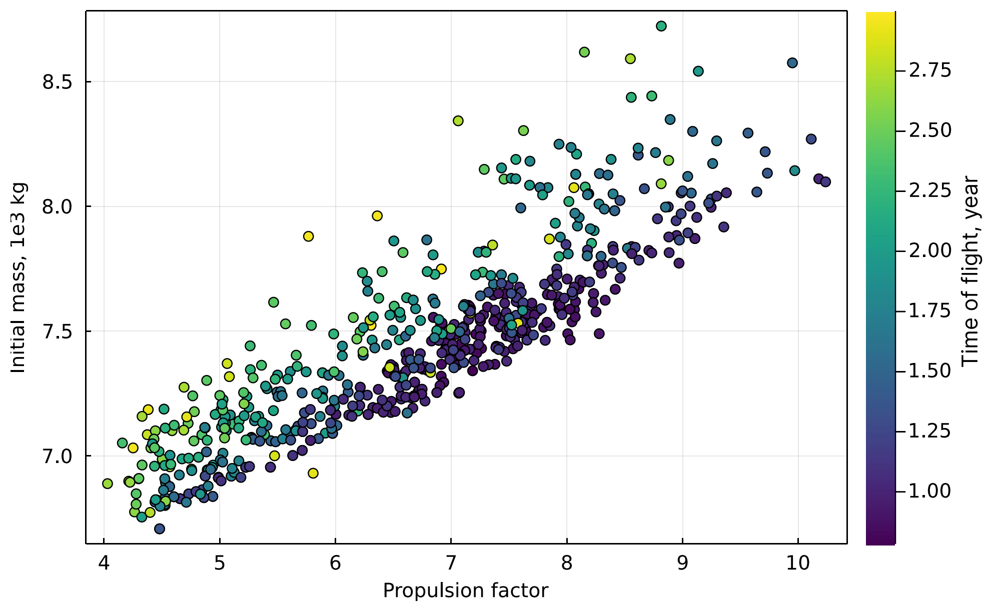

Figure 4: IMLEO against propulsion factor s

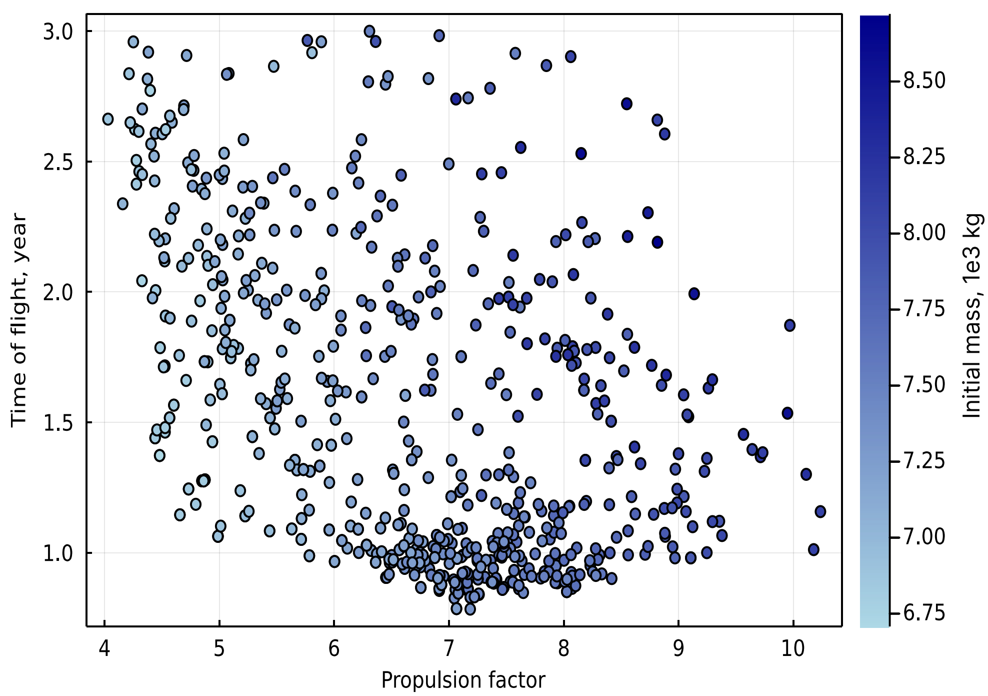

Figure 5: Time of flight against propulsion factor s

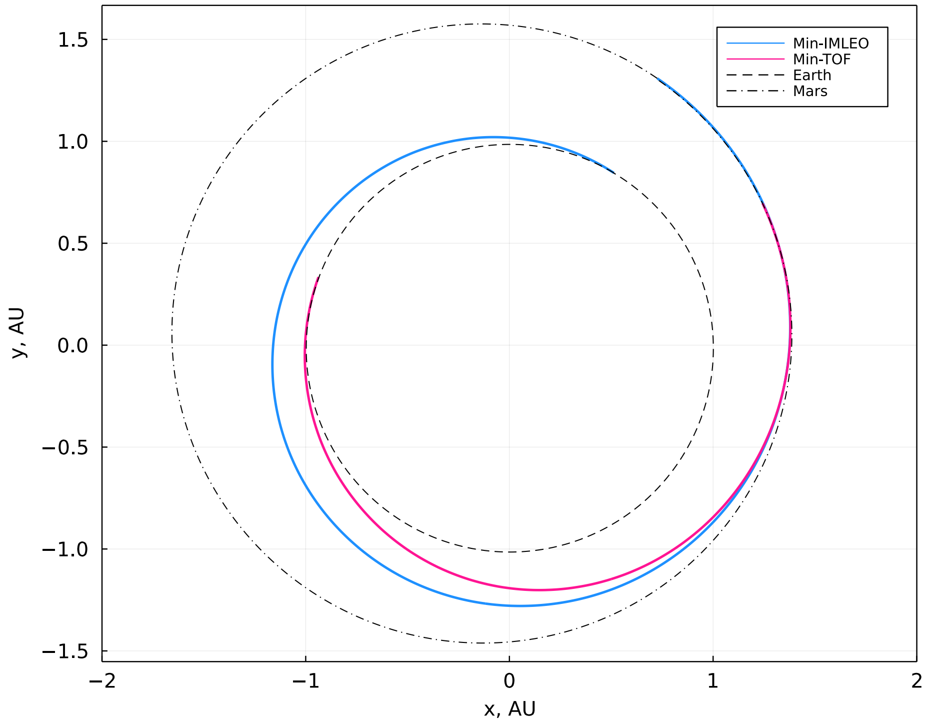

Figure 6: Optimal trajectories corresponding to minimum IMLEO and minimum TOF

CONCLUSION

This work explored a novel optimization formulation that simultaneously considers the trajectory of a low-thrust interplanetary spacecraft with SEP. The Sims-Flanagan transcription has been extended to also include variables dictating the size and performance of the power and propulsion subsystems, as well as the mode on the power at which the propulsion system is to be operated at a given time along the transfer. Compared to trajectory-only problem formulations, the introduced method can identify the scale of the SEP system necessary to meet mission objectives such as payload mass and time of flight. Furthermore, it provides insight into the trade-off between the trajectory and the spacecraft design itself along Pareto fronts having direct consequences to the high-level mission design. This enables a concurrent trade-off of both the spacecraft trajectory and the vehicle sizing. As the frontier of both human and robotic space exploration expands, increased carrying capacity enabled by SEP will become an indispensable piece of logistics, and the proposed analysis provides a quantitative approach for considering different mission designs.

REFERENCES

[1] T. E. Hammel, R. Bennett, W. Otting, and S. Fanale, "Multi-Mission Radioisotope Thermoelectric Generator (MMRTG) and performance prediction model," *7th International Energy Conversion Engineering Conference*, No. August, 2009, 10.2514/6.2009-4576.

[2] J. Kawaguchi, A. Fujiwara, and T. Uesugi, "Hayabusa - Its technology and science accomplishment summary and Hayabusa-2," *AIAA 57th International Astronautical Congress, IAC 2006*, Vol. 2, 2006, pp. 1210–1216, 10.2514/6.iac-06-a3.5.02.

[3] Y. Tsuda, T. Saiki, N. Ogawa, and M. Morimoto, "Trajectory Design for Japanese New Asteroid Sample Return Mission Hayabusa-2," *International Symposium on Space Flight Dynamics*, No. 1, 2012, pp. 1–7.

[4] R. Jehn, S. Campagnola, D. Garcia, and S. Kemble, “Low-thrust approach and gravitational capture at Mercury,” *European Space Agency, (Special Publication) ESA SP*, No. 548, 2004, pp. 487–492.

[5] D. G. Yarnoz, R. Jehn, and P. De Pascale, “Trajectory design for the Bepi-Colombo mission to mercury,” *57th International Astronautical Congress*, Vol. 7, 2006, pp. 4712–4719, 10.2514/6.iac-06-c1.8.07.

[6] D. Y. Oh, D. Goebel, B. Hart, G. Lantoine, J. S. Snyder, and Whiffen, “Development of the Psyche Mission for NASA’s Discovery Program,” *International Electric Propulsion Conference*, Atlanta, 2017, p. 153.

[7] H. Toyota, K. Nishiyama, Y. Kawakatsu, S. Sato, T. Yamamoto, S. Okazaki, T. Nakamura, R. Funase, T. Inamori, T. Arai, K. Ishibashi, M. Kobayashi, and , “DESTINY + : Deep Space Exploration Technology Demonstrator and Explorer to Asteroid 3200 Phaethon,” *Low-Cost Planetary Missions Conference*, 2017, pp. 1–23.

[8] E. N. A. o. Sciences and Medicine, *Origins, Worlds, and Life: A Decadal Strategy for Planetary Science and Astrobiology 2023-2032*. Washington, DC: The National Academies Press, 2022, 10.17226/26522.

[9] M. Isaji, Y. Takubo, and K. Ho, “Multidisciplinary Design Optimization Approach to Integrated,” *Journal of Spacecraft and Rockets*, 2022, pp. 1–11, 10.2514/1.A35284.

[10] A. K. Nicholas, R. C. Woolley, A. Didion, F. Laipert, Z. Olikara, R. Webb, and R. Lock, “Simultaneous optimization of spacecraft and trajectory design for interplanetary missions utilizing solar electric propulsion,” *AAS/AIAA Space Flight Mechanics Meeting*, Vol. 168, 2019, pp. 2855–2871.

[11] V. G. Petukhov and W. S. Wook, “Joint Optimization of the Trajectory and the Main Parameters of an Electric Propulsion System,” *Procedia Engineering*, Vol. 185, 2017, pp. 312–318, 10.1016/j.proeng.2017.03.309.

[12] V. Arya, E. Taheri, and J. L. Junkins, “A composite framework for co-optimization of spacecraft trajectory and propulsion system,” *Acta Astronautica*, Vol. 178, 2021, pp. 773–782, https://doi.org/10.1016/j.actaastro.2020.10.007.

[13] S. Ceccherini, K. V. Mani, and F. Topputo, “Combined System – Trajectory Design for Geostationary Orbit Platforms on Hybrid Transfer,” *Journal of Spacecraft and Rockets*, 2021, pp. 1–19, 10.2514/1.A35012.

[14] E. Taheri, “Low-thrust trajectory design using multi-mode propulsion systems: A grid-based thruster model,” *AIAA Scitech 2020 Forum*, Vol. 1 PartF, No. January, 2020, pp. 1–18, 10.2514/6.2020-2183.

[15] V. Arya, E. Taheri, and J. Junkins, “Electric thruster mode-pruning strategies for trajectory-propulsion co-optimization,” *Aerospace Science and Technology*, Vol. 116, 2021, p. 106828, 10.1016/j.ast.2021.106828.

[16] J. A. Sims and N. Flanagan, “Preliminary design of low-thrust interplanetary missions,” *AAS Astrodynamics Specialists Conference*, 1999.

[17] T. T. McConaghy, T. J. Debban, A. E. Petropoulos, and J. M. Longuski, “Design and optimization of low-thrust trajectories with gravity assists,” *Journal of Spacecraft and Rockets*, Vol. 40, No. 3, 2003, pp. 380–387, 10.2514/2.3973.

[18] C. H. Yam, D. Izzo, and D. D. Lorenzo, “Low-thrust trajectory design as a constrained global optimization problem,” *Proceedings of the Institution of Mechanical Engineers, Part G: Journal of Aerospace Engineering*, Vol. 225, No. 11, 2011, pp. 1243–1251, 10.1177/0954410011401686.

[19] Y. Shimane and K. Ho, “Robustness Assessment of Low-Thrust Trajectory via Sequentially Truncated Sims-Flanagan Problems,” *AIAA ASCEND*, Las Vegas, 2021, pp. 1–16, 10.2514/6.2021-4153.

[20] J. A. Englander and B. A. Conway, “Automated solution of the low-thrust interplanetary trajectory problem,” *Journal of Guidance, Control, and Dynamics*, Vol. 40, No. 1, 2017, pp. 15–27, 10.2514/1.G002124.

[21] M. W. Crofton, J. E. Pollard, E. J. Beiting, R. Spektor, K. D. Diamant, X. L. Eapen, R. B. Cohen, and M. J. Patterson, “Characterization of the NASA NEXT thruster,” *45th AIAA/ASME/SAE/ASEE Joint Propulsion Conference and Exhibit*, No. August, 2009, 10.2514/6.2009-4815.

[22] P. Saripalli, E. Cardiffy, and J. Englander, “NEXT performance curve analysis and validation,” *52nd AIAA/SAE/ASEE Joint Propulsion Conference, 2016*, No. Code 597, 2016, pp. 1–30.

[23] P. E. Gill, W. Murray, and M. A. Saunders, “SNOPT: An SQP algorithm for large-scale constrained optimization,” *SIAM Review*, Vol. 47, No. 1, 2005, pp. 99–131, 10.1137/S0036144504446096.

[24] A. Wächter and L. T. Biegler, “On the implementation of an interior-point filter line-search algorithm for large-scale nonlinear programming,” *Mathematical Programming*, Vol. 106, No. 1, 2006, pp. 25–57, 10.1007/s10107-004-0559-y.

[25] D. J. Wales and J. Doye, “Global Optimization by Basin-Hopping and the Lowest Energy Structures of Lennard-Jones Clusters Containing up to 110 Atoms,” *The Journal of Physical Chemistry A.*, Vol. 101, No. 28, 1997, pp. 5111–5116.

[26] C. H. Yam, D. Izzo, and D. D. Lorenzo, "Low-thrust trajectory design as a constrained global optimization problem," *Proceedings of the Institution of Mechanical Engineers, Part G: Journal of Aerospace Engineering*, Vol. 225, No. 11, 2011, pp. 1243–1251, 10.1177/0954410011401686.

[27] D. Izzo, "PyGMO and PyKEP: open source tools for massively parallel optimization in astrodynamics (the case of interplanetary trajectory optimization)," *5th International Conference Astrodynamics Tools and Techniques*, 2012.

[28] J. A. Englander and A. C. Englander, "Tuning Monotonic Basin Hopping: Improving the Efficiency of Stochastic Search as Applied to Low-Thrust Trajectory Optimization," *International Symposium on Space Flight Dynamics*, 2014, pp. 1–33.

[29] S. L. McCarty and M. L. McGuire, "Parallel monotonic basin hopping for low thrust trajectory optimization," *Space Flight Mechanics Meeting, 2018*, No. 210009, 2018, 10.2514/6.2018-1452.

[30] Y. Shimane and K. Ho, "Gravity-Assist Low-Thrust Inter-System Trajectory Design with Manifold Captures," *The Journal of the Astronautical Sciences*, 2022, 10.1007/s40295-022-00319-x.